Available online at www.sciencedirect.com
SCIENCE DIRECT®
Earth and Planetary Science Letters 248 (2006) 77–89
EPSL
www.elsevier.com/locate/epsl

Subsolidus phase relations and perovskite compressibility in the system $MgO–AlO_{1.5}–SiO_2$ with implications for Earth's lower mantle

Michael J. Walter [a,*], Reidar G. Trønnes [b], Lora S. Armstrong [a], Oliver T. Lord [a], Wendel A. Caldwell [c], Simon M. Clark [c]

[a] *Department of Earth Sciences, University of Bristol, Wills Memorial Building, Queen's Rd., Bristol, BS8 1RJ, United Kingdom*
[b] *Natural History Museum, Geology, University of Oslo, Box 1172, Blindern, 0318 Oslo, Norway*
[c] *Advanced Light Source, Lawrence Berkeley National Laboratory, Berkeley, California 20015, USA*

Received 22 February 2006; received in revised form 12 May 2006; accepted 14 May 2006
Available online 30 June 2006
Editor: G. D. Price

Abstract

Experimentally determined phase relations in the system $MgO–AlO_{1.5}–SiO_2$ at pressures relevant to the upper part of the lower mantle indicate that Mg–silicate perovskite incorporates aluminum into its structure almost exclusively by a charge-coupled reaction. $MgSiO_3$-rich bulk compositions along the joins $MgSiO_3–MgAlO_{2.5}$ and $MgSiO_3–MgAl_2O_4$ crystallize assemblages of perovskite coexisting with periclase. MgO-saturated perovskites along these joins have ambient unit cell volumes consistent with those measured and calculated for aluminous perovskite along the charge-coupled substitution join, $MgSiO_3–AlO_{1.5}$. The compressibility of aluminous perovskite along the MgO-saturated joins is not anomalously low as predicted for oxygen-defect perovskites. The bulk moduli, however, are consistent with previous measurements made for aluminous perovskites along the charge-coupled substitution join. These results agree with first-principles calculations showing very limited stability of O-defects in Mg-perovskite at pressures and temperatures corresponding to lower mantle conditions, but are inconsistent with earlier experimental results showing unusually compressive aluminous perovskite. The maximum solubility of alumina in perovskite is ~25 mol% along the $MgSiO_3–AlO_{1.5}$ join within the ternary MAS-system (i.e. pyrope composition), and the join is apparently binary. Although primitive mantle peridotite compositions are MgO-saturated and fall nearly on the oxygen vacancy join, alumina substitution into perovskite is expected to occur primarily by charge-coupled substitution throughout the lower mantle. The compressibility of aluminous perovskite in primitive mantle is expected to be only a few percent lower than for end member $MgSiO_3$ perovskite.

Keywords: perovskite; lower mantle; alumina substitution; bulk modulus; oxygen vacancy; defects

1. Introduction

Quantifying the mineralogy of Earth's lower mantle requires accurate knowledge of the phase relations and thermoelastic properties of its constituent phases [1,2]. One of the most important parameters is the compressibility (β), or in more conventional terms the inverse of this parameter, the incompressibility or bulk modulus (K). This is because the bulk modulus relates in a relatively simple way to the most well-constrained observations available about the lower mantle, the velocity of

* Corresponding author. Tel.: +44 117 331 5007; fax: +44 117 925 3385.
E-mail address: m.j.walter@bristol.ac.uk (M.J. Walter).

0012-821X/$ - see front matter © 2006 Elsevier B.V. All rights reserved.
doi:10.1016/j.epsl.2006.05.017

compressional seismic waves and the density. The compressibility is also the simplest elastic parameter to measure in the laboratory. Models derived from laboratory measurements of elastic parameters indicate that magnesium silicate perovskite constitutes some 70 vol.% of the lower mantle, an amount generally consistent with a mineralogy that can be produced by a bulk composition similar to primitive upper mantle, or 'pyrolite' [1–3].

Observations from four experimental studies indicate that values for the bulk modulus of $MgSiO_3$ perovskite typically used in mineralogic models, about 260 GPa, may be considerably too high [4–7]. These studies indicate that even the small amount of Al_2O_3 in a pyrolite mantle, about 5 mol%, can cause about a 10% reduction in the bulk modulus when substituted into perovskite. If true, previous models for lower mantle mineralogy based on the higher bulk modulus become erroneous, and the geochemically comfortable model of a pyrolitic lower mantle, dubious.

This state of affairs has created a flurry of activity, both experimental and theoretical, to understand how aluminum substitutes into the perovskite structure, and how that substitution affects the compressibility [7–16]. Although results from these studies are not in uniform agreement, it has emerged that the substitution mechanism is likely to control the compressibility. Two simple substitution mechanisms are critical in this sense. The first is a charge-coupled substitution in which two Al^{3+} cations substitute for one Mg^{2+} in approximately 8-fold coordination (A-site) and one Si^{4+} in 6-fold coordination (B-site):

$$Al^{3+}[VIII] + Al^{3+}[VI] \leftrightarrow Mg^{2+}(VIII) + Si^{4+}[VI] \quad (1)$$

The second is a different kind of substitution in which an oxygen vacancy (V_0), or 'O-defect', is created in the structure to maintain charge balance. In this case, two Al^{3+} cations substitute for two Si^{4+} in 6-fold coordination:

$$Al^{3+}[VI] + V_0 \leftrightarrow 2Si^{4+}[VI] + O^{2-} \quad (2)$$

Fig. 1 shows these substitution mechanisms chemographically in the ternary system $MgO–AlO_{1.5}–SiO_2$. The first reaction corresponds to the join $MgSiO_3–AlO_{1.5}$ (charge-coupled join), and the second reaction to the join $MgSiO_3–MgAlO_{2.5}$ (O-defect join).

Theoretical calculations show that these two substitution mechanisms will have distinctly different effects on the compressibility of perovskite [9,10,12]. Charge-coupled substitution should have only a mild effect when compared to aluminum-free perovskite, producing a somewhat softer structure. In contrast, the formation of oxygen vacancies has a more profound effect, causing a considerable softening of the structure even for modest amounts of aluminum substitution. Experimental evidence could be interpreted to confirm this dichotomy. Andrault et al. [8] and Walter et al. [14] have measured the compressibilities of a series of aluminous perovskites along the charge-coupled join, and observed only a mild effect on the bulk modulus generally consistent with theoretical calculations. Navrotsky et al. [17] synthesized perovskites along the O-defect join, as well as other MgO-saturated perovskite compositions. Based on interpreted phase relations as well as thermochemical measurements, these authors postulated that the O-defect substitution mechanism is competitive with the charge-coupled mechanism for MgO-rich compositions. Further, Walter et al. [14] noted that the earlier experimental results showing unusually compressive aluminous perovskites are remarkably consistent with theory if alumina substitutes by the O-defect forming reaction.

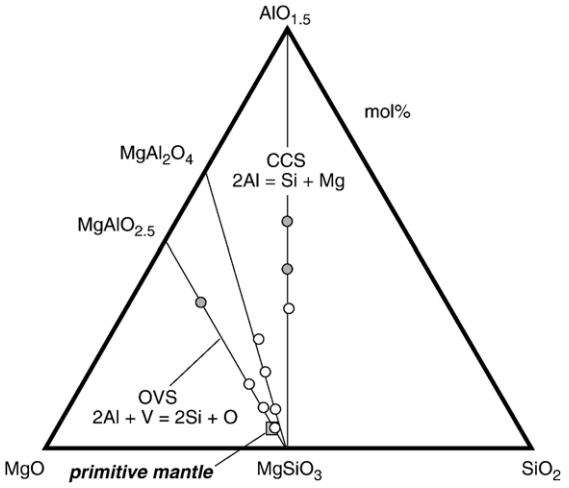

Fig. 1. The system $MgO–AlO_{1.5}–SiO_2$ (mol%, MAS). The join $MgSiO_3–AlO_{1.5}$ represents a charge-coupled substitution reaction (CCS), and the join $MgSiO_3–MgAlO_{2.5}$ represents an oxygen vacancy substitution reaction (OVS). White circles show the measured compositions of glass starting materials, whereas the shaded circles show the weighed compositions of oxide starting compositions. The shaded square shows a pyrolitic primitive mantle composition projected into the MAS-system.

The relative importance of the two substitution mechanisms in lower mantle perovskites is still unresolved. Compositional models of fertile mantle, such as pyrolite, fall to the MgO-rich side of the charge coupled and the O-defect substitution joins but relatively close to the O-defect join (Fig. 1). Therefore, if the O-defect component is stable at lower mantle conditions, even to a very modest degree, the MgO-saturated mantle perovskite may be

much more compressible than previously considered. Theoretical calculations indicate that the O-defect component should not be stable at lower mantle conditions of pressure and temperature because pressure has a de-stabilizing effect on oxygen vacancy formation [9,10,12,18,19]. However, to date there has been no unambiguous experimental confirmation of the theoretical results and, if the previous experiments showing anomalously compressive perovskites are indicative, perovskite with considerable amounts of oxygen defects might be stable at lower mantle conditions.

Here, we present new results for the phase relations and compressibility of aluminous perovskites along the MgO-saturated joins $MgSiO_3$–$MgAlO_{2.5}$ and $MgSiO_3$–$MgAl_2O_4$. We synthesized a series of perovskites at conditions corresponding to the upper part of the lower mantle using the laser-heated diamond anvil cell, and determined phase relations using synchrotron-based X-ray diffraction. We then determined the compressibility of selected samples on each join. We find that the bulk of the evidence does not support significant substitution of alumina by formation of oxygen vacancies in mantle perovskite, and that the compressibility of aluminous perovskite in the mantle should be very close to Al-free perovskite.

2. Experimental methods

We made ten starting compositions in the system MgO–$AlO_{1.5}$–SiO_2 as shown on Fig. 1 and listed in Table 1. About 1 g of each starting mixture was measured using oxide components, with each oxide measured to a precision of better than 0.1 mg. Seven of these mixtures were loaded into Pt capsules and fused in air at 1 atm, 1700 °C for 1.5–2 h in a vertical tube furnace and drop quenched into water. Optical microscopy and back-scattered electron imaging did not reveal any crystals or crystallites. Electron microprobe analyses of the glasses are provided in Table 1, and measured oxide compositions show low standard errors of the mean indicating homogeneity on a micron scale. Glasses were pulverized to a fine powder in an agate mortar. About 10 wt.% Pt black was added to powdered mixtures to act as a laser absorber, as well as a pressure standard in compression experiments. The glass + Pt powders were then ground to micron or sub-micron size, which helps to assure uniform heating. The other three oxide compositions were too refractory to melt in our furnace and so we made experiments directly with the oxide mixtures. About 10 wt.% Pt black was added and the powders pulverized. All powders were dried at 120 °C and stored in a desiccator to prevent adsorption of water. However, it is likely given the fine particle size of the powders, that some unquantified amount of water remains adsorbed to particles [20].

High-pressure synthesis experiments were made using symmetric piston-cylinder type diamond anvil cells using diamonds with 200 to 300 μm flat culets. Powdered samples were loaded into a 100 μm diameter sample chamber drilled into a pre-indented stainless steel gasket. No pressure medium was used in the synthesis experiments to assure compositional integrity. Pressure is determined using the ruby fluorescence method [21]. However, because of possible contamination of the sample by the ruby (Cr-doped Al_2O_3), a small ruby chip was placed just at the edge of the sample chamber but on the gasket. The sample was compressed such that the ruby yielded a

Table 1
Compositions of starting materials

Mixture	Composition (mol%)	Type	*n*	Measured [a] (wt.%)			
				MgO	Al_2O_3	SiO_2	Total
E	$90MgSiO_3$–$10MgAlO_{2.5}$	Glass	40	40.19 (4) [b]	5.25 (3)	54.40 (7)	99.84 (10)
I	$80MgSiO_3$–$20MgAlO_{2.5}$	Glass	40	40.53 (16)	10.51 (4)	49.05 (5)	100.09 (18)
K	$70MgSiO_3$–$30MgAlO_{2.5}$	Glass	40	40.82 (17)	15.97 (5)	43.13 (6)	99.92 (20)
OMA	$30MgSiO_3$–$70MgAlO_{2.5}$	Oxide	–	42.87	37.96	19.17	100.0
F	$90MgSiO_3$–$10MgAl_2O_4$	Glass	40	38.45 (18)	9.9 (4)	51.91 (5)	100.29 (20)
G	$80MgSiO_3$–$20MgAl_2O_4$	Glass	40	37.02 (17)	18.88 (5)	44.31 (5)	100.23 (19)
L	$70MgSiO_3$–$30MgAl_2O_4$	Glass	40	35.19 (11)	27.25 (4)	37.24 (5)	99.68 (11)
O	$67MgSiO_3$–$33AlO_{1.5}$	Glass	10	25.96 (11)	33.24 (7)	39.72 (21)	98.95 (14)
OMC	$57MgSiO_3$–$43AlO_{1.5}$	Oxide	–	22.79	43.24	33.97	100.0
OMD	$45MgSiO_3$–$55AlO_{1.5}$	Oxide	–	17.91	55.38	26.71	100.0

[a] Oxide concentration in glasses as measured by EPMA (weight percent). Analysis performed using wavelength dispersive spectroscopy, a 15 kV potential, and a 20 nA beam current, and silicate and oxide standards. Raw counts were converted to oxide concentration using a ZAF correction scheme. Glasses were found to contain ~0.3 wt.% contaminant CaO, which was traced to the MgO oxide. Oxide mix concentrations based on weighed amounts.

[b] Two standard errors of the mean in the least significant digits.

pressure of ~30–35 GPa before heating in most experiments. Based on calibration of this arrangement, the pre-heating pressure in the center of the hole would have been of the order 40–50 GPa. Further, based on runs with ruby grains placed within the heated region, relaxation of pressure during heating of the sample typically results in a decrease in peak pressure after heating of ~5–10 GPa. We have assigned a conservative estimate of uncertainty of ±10 GPa in these experiments. Table 2 gives estimated conditions for all experiments.

Samples were heated with a 50 W, diode-pumped Nd–YLF laser operating in TEM_{01} mode and using a double-sided heating geometry. Although large temperature gradients are always present at the edges of the circular heated region, this heating geometry promotes uniform heating both radially and axially within the heated region [22,23]. Temperature was measured on one side using conventional spectroradiometric techniques as described in detail elsewhere [24]. Two heating styles were used, and duplicate syntheses were made on most compositions. In one heating style (type A, Table 2), a 20–30 μm spot was used, and the laser was slowly scanned across the sample and laser power was modulated to achieve a maximum temperature close to 2500 K throughout the sample. The sample edge was avoided to assure no reaction with the gasket or ruby grain. Typical uncertainty on the peak temperature of any given spot is less than 50 K based on fits to the Planck spectrum. However, a heated spot would typically have temperature fluctuations of at least 50 K due to irregular absorptions of the laser energy. In the worst cases this would reach several hundred degrees. Thus, a general temperature uncertainty of ±200–300 K across the sample is estimated for this heating style. The sample was heated in this way for 30 min.

In duplicate experiments we used an alternate heating style, type B. We targeted a maximum temperature of 2000 K and used a broad beam 40–50 μm in diameter. The temperature uncertainty tended to be less severe in these experiments as broad-beam heating at lower temperatures produced less overall temperature irregularity within the heated region. The broad beam was placed in one position for tens of minutes at a time. The entire sample chamber was covered with overlap between each heating region while avoiding the sample edges. Total heating times were 60–70 min.

Phase identification and measurement of unit cell parameters of phases in pressure and temperature quenched samples were made by X-ray diffraction at beamline 12.2.2 of the Advanced Light Source, Lawrence Berkeley National Lab. Angle dispersive diffraction was made using a MAR345 imaging plate, with an incident X-ray at a wavelength of 0.6199 Å (20 keV) focused with a set of KB mirrors to a beam diameter of ~20 μm. Sample to detector distance was calculated using a LaB_6 standard. Reproduction of sample to detector distance between experiments was <10 μm based on repositioning of samples to the stage rotation center. Two-dimensional diffraction images were reduced to intensity -2θ plots using FIT2D software [25]. Unit cell refinements were made using the Celref program [26]. Three to five diffraction patterns were taken from each sample and acquisition times were typically 300 s.

We made compression experiments on two synthesized samples (Exp37 and Exp52, Table 2). Sample pellets ~80 μm in diameter and 15 μm thick were removed from their gaskets. Each sample was then inserted into a 100 μm hole of a freshly drilled gasket pre-indented to a thickness of ~50 μm. A 4:1 methanol–ethanol mixture was used as a hydrostatic pressure medium. Samples were compressed and diffraction data taken at high pressures using an X-ray with a wavelength of 0.4133 Å (30 keV). Sample pressure was determined from the unit cell volume of Pt using the equation-of-state of Holmes [27]. We found that the pressure medium remained liquid (hydrostatic) up to about 15 GPa, indicating the presence of a small amount of water in the mixture. In one experiment pressure reached about 18 GPa and the pressure medium stiffened upon solidification. This caused considerable

Table 2
Experimental specifications

Starting mix	Exp. #	P (GPa)	T (K)	Heat style[a]	Duration (min)	Phases[b]
E	25	40 (10)[c]	2500 (200)	A	30	Pv, per
E	34	40 (10)	2000 (200)	B	60	Pv, per
I	26	40 (10)	2300 (300)	A	30	Pv, per
I	37	40 (10)	2000 (300)	B	60	Pv, per
K	27	40 (10)	2300 (300)	A	30	Pv, per
K	40	40 (10))	2000 (200)	B	60	Pv, per
OMA	21	40 (10))	2400 (400)	A	10	Pv, per, CF
F	28	40 (10)	2300 (300)	A	30	Pv, per
F	52	40 (10)	2100 (300)	B	70	Pv, per
G	29	40 (10)	2300 (200)	A	35	Pv, per
G	31	40 (10)	1800 (300)	B	60	Pv, per
L	35	40 (10)	2300 (200)	A	30	Pv, per, CF
L	46	40 (10)	2000 (200)	B	70	Pv, per, CF
O	61	55 (10)	2000 (300)	A	30	Pv, cor
OMC	5	45 (10)	2300 (200)	A	20	Pv, cor
OMD	6	40 (10)	2000 (500)	A	20	Pv, cor

[a] Heating styles as described in Section 2.1.
[b] Phases observed by X-ray diffraction. Pv=perovskite; per=periclase; CF=calcium ferrite or calcium titanate structured phase of $MgAl_2O_4$.
[c] Estimated uncertainty as explained in Section 2.1.

broadening of perovskite peaks. To mitigate against stress accumulation we heated the entire DAC with a hot air gun for several minutes until the cell was too hot to handle (e.g. several hundreds of °C). Then the perovskite peaks became considerably sharper, permitting determination of a reasonably precise cell volume.

3. Results

3.1. Phase relations

An important question with respect to the petrology of the lower mantle is whether Mg-perovskite can accommodate oxygen defects to a considerable degree. That is, does solid solution of Al^{3+} via reaction (2) along the join $MgSiO_3$–$MgAlO_{2.5}$ occur to a degree sufficient to have an important effect on elastic properties? For example, solution of only about 10 mol% $MgAlO_{2.5}$ into $MgSiO_3$ perovskite would constitute a fully O-defect perovskite in primitive mantle composition (Fig. 1). Navrotsky et al. [17] reported the possible incorporation of O-defects in perovskite in a composition with ~10 mol% $AlO_{1.5}$ along the $MgSiO_3$–$MgAlO_{2.5}$ join. According to theoretical calculations this could reduce the bulk modulus by at least 10% [9]. As pointed out by Navrotsky et al. [17] and by Walter et al. [14], a ternary solid solution between the joins $MgSiO_3$–$AlO_{1.5}$ and $MgSiO_3$–$MgAlO_{2.5}$ is plausible and the phase boundary may not extend all the way to the O-defect join. This seems to be supported by the thermochemical results of Navrotsky et al. [17]. In contrast, recent theoretical calculations [12] indicate that negligible amounts of O-defects can be accommodated in aluminous perovskite at lower mantle pressures and temperatures, generally consistent with predictions from previous theoretical work [9,18]. Akber-Knutsen and Bukowinski [12] concluded that O-vacancy substitution may account for only 3–4% and less than 1% of the Al-substitution in the uppermost and the deeper parts of the lower mantle, respectively.

As a first test for the solubility mechanism of alumina in perovskite we look at the phase relations in our synthesis experiments. Our simple procedure is illustrated in Fig. 2. If reaction (2) operates along the $MgSiO_3$–$MgAlO_{2.5}$ join then a single phase of Mg-perovskite should appear in our experiments. Likewise, if a ternary perovskite is stable between the joins $MgSiO_3$–$AlO_{1.5}$ and $MgSiO_3$–$MgAlO_{2.5}$, for example along $MgSiO_3$–$MgAl_2O_4$, then a single phase of perovskite should be present. However, if O-defects are unstable in perovskite, as indicated by theory, then we should expect a two-phase assemblage of perovskite+periclase to occur along these joins. Tie lines extending from the MgO apex through our bulk compositions along these joins reveal that MgO should vary from about 5 to 14 mol% for these compositions (Fig. 2).

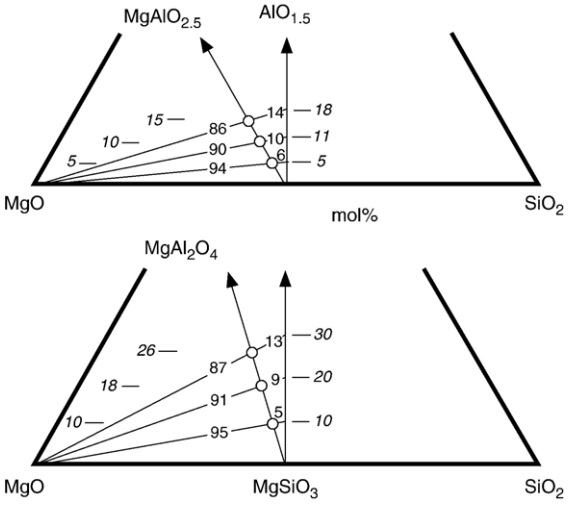

Fig. 2. Diagrams illustrating use of the lever rule for deducing phase relations in the system MgO–$AlO_{1.5}$–SiO_2. If O-defects are not stable in perovskite along the $MgSiO_3$–$MgAlO_{2.5}$ and $MgSiO_3$–$MgAl_2O_4$ joins, then perovskite and periclase will crystallize together, with their relative proportions determined by the level rule. The amount of periclase should increase as compositions move away from $MgSiO_3$ as shown. Italicized numbers to the left of the $MgSiO_3$–$MgAlO_{2.5}$ and $MgSiO_3$–$MgAl_2O_4$ joins give $AlO_{1.5}$ contents of the starting mixtures, whereas those on the right side of the diagram give projected $AlO_{1.5}$ contents along the $MgSiO_3$–$AlO_{1.5}$ join.

The phases present in our experiments as revealed by X-ray diffraction are given in Table 2. Perovskite is present in every experiment, and the overall high quality of the diffraction patterns, an example of which is shown in Fig. 3, indicate well crystallized samples. We observe evidence for MgO (periclase) in all experiments along the $MgSiO_3$–$MgAlO_{2.5}$ and $MgSiO_3$–$MgAl_2O_4$ joins. Fig. 4 shows diffraction peaks in the region of the most intense periclase reflection {200} for a sequence of compositions along the $MgSiO_3$–$MgAlO_{2.5}$ join with 10, 20 and 30 mol% $MgAlO_{2.5}$. The {200} reflection is already apparent in the composition with only 10 mol% $MgAlO_{2.5}$, implying that a single defect perovskite is not stable even in this relatively low alumina composition. Further, the magnitude of the {200} reflection increases as the amount of $MgAlO_{2.5}$ increases in the bulk composition, just as it should according to the tie lines in Fig. 2 if this join lies within a 2-phase region where perovskite and periclase are stable. The {200} reflection becomes obscured by and merges into the perovskite {121} reflection as the $AlO_{1.5}$ content of the compositions increase. This occurs because as $AlO_{1.5}$ dissolves into perovskite its structure becomes

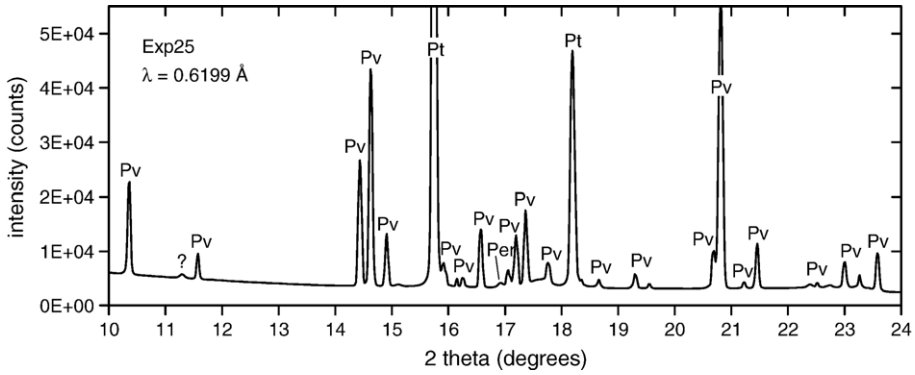

Fig. 3. Example diffraction pattern taken at ambient conditions from sample Exp25 (Table 2) for a composition with 5 mol% $AlO_{1.5}$ along the $MgSiO_3$–$MgAlO_{2.5}$ join. Peak labels are Pv=perovskite, Per=periclase, and Pt=platinum. The diffraction pattern was acquired for 300 s with an X-ray wavelength of 0.6199 Å.

progressively distorted, and the changes in unit cell parameters cause progressively larger cell volumes [8,14,28,29]. Periclase peaks were also evident along the $MgSiO_3$–$MgAl_2O_4$ join, although the sequence of increasing {200} peak intensity was not as discernable as along the $MgSiO_3$–$MgAlO_{2.5}$ join. We note also that the weaker {220} periclase reflection was evident in many spectra. Our interpretation of the spectra is that periclase is a stable phase along both joins at the conditions of our experiments (e.g. ~40 GPa, 2000–2500 K). This evidence is circumstantial in that we presume that the observed two-phase assemblages represent equilibrium. These experiments are not reversed, and periclase could crystallize as a metastable phase during heating. The lack of periclase in spectra along the join $MgSiO_3$–$AlO_{1.5}$ [14] and the systematic increase of the intensity of the periclase {200} peak along the $MgSiO_3$–$MgAlO_{2.5}$ join as predicted from phase relations, however, provides support for our interpretation.

In the composition with 70 mol% $MgAlO_{2.5}$ we observe weaker perovskite peaks and many new peaks that can be associated with high pressure forms of $MgAl_2O_4$ in both the Ca ferrite (CF) and Ca titanite (CT) structures [30]. We note that our experimental pressure was close to the Ca ferrite and Ca titanite transition in $MgAl_2O_4$ [30]. This implies that the composition with 70 mol% $MgAlO_{2.5}$ resides within the three-phase region perovskite+periclase+$MgAl_2O_4$ (CF or CT). We also observe the emergence of several new weak diffraction peaks in the composition with 30 mol% $MgAl_2O_4$ along the $MgSiO_3$–$MgAl_2O_4$ join that also can generally be assigned to high pressure $MgAl_2O_4$ phases, suggesting this composition lies just within a three-phase field.

We made several experiments along the join $MgSiO_3$–$AlO_{1.5}$ in order to locate the maximum solubility of $AlO_{1.5}$ in perovskite (Table 2). We found that perovskite coexists with corundum in all three compositions spanning a range of 33 to 55 mol% $AlO_{1.5}$. The starting composition with

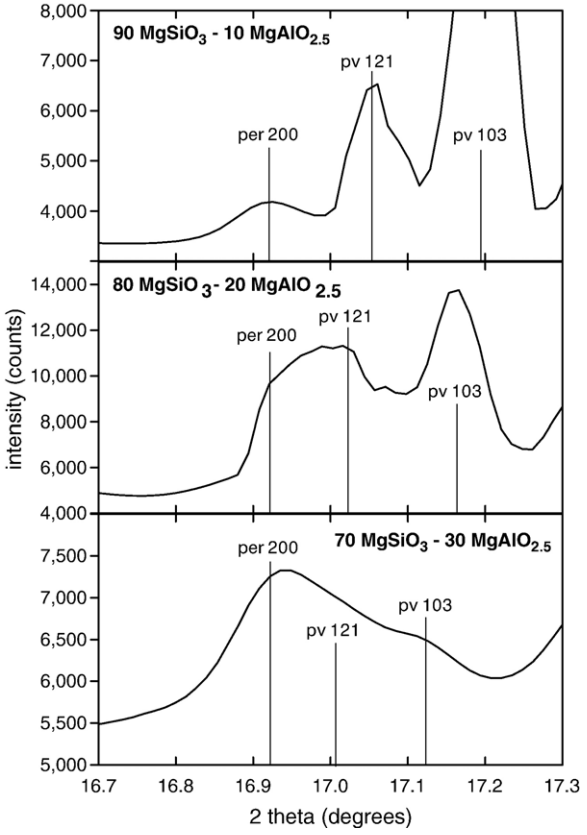

Fig. 4. Diffraction patterns from 16.7° to 17.3° 2θ for samples synthesized along the $MgSiO_3$–$MgAlO_{2.5}$ join. Note the clear presence of the periclase {200} reflections even in the composition with only 5 mol% alumina. The {200} reflection appears to increase in intensity relative to surrounding perovskite peaks as the amount of alumina increases in the bulk composition.

Table 3
Unit cell volume of aluminous perovskites at 1 atm, 273 K

Exp. #	Mixture	a (Å)	b (Å)	c (Å)	V_0 (Å^3)
25	E	4.7786 (10)[a]	4.9326 (7)	6.9045 (18)	162.75 (6)
34	E	4.7781 (8)	4.9338 (6)	6.9086 (10)	162.87 (4)
37	I	4.7771 (17)	4.9385 (14)	6.9167 (23)	163.18 (9)
27	K	4.7850 (9)	4.9432 (10)	6.9376 (30)	164.10 (9)
40	K	4.7851 (11)	4.9437 (12)	6.9389 (23)	164.15 (8)
28	F	4.7789 (6)	4.9380 (9)	6.9219 (16)	163.35 (6)
52	F	4.7793 (13)	4.9369 (9)	6.9192 (17)	163.26 (9)
29	G	4.7837 (14)	4.9434 (14)	6.9313 (36)	163.91 (11)
31	G	4.7860 (28)	4.9449 (30)	6.9212 (62)	163.80 (20)
35	L	4.7886 (19)	4.9508 (15)	6.9578 (31)	164.95 (11)
46	L	4.7854 (22)	4.9541 (46)	6.9358 (59)	164.43 (22)
61	O	4.7814 (14)	4.9500 (21)	6.9667 (33)	164.89 (14)
5	OMC	4.7837 (14)	4.9515 (19)	6.9439 (60)	164.48 (16)
6	OMD	4.7852 (27)	4.9495 (20)	6.9557 (87)	164.74 (23)

[a] Uncertainty is one standard error in least significant digits based on unit cell refinement.

33% $AlO_{1.5}$ was a glass, and so the presence of corundum in this composition is particularly constraining. The strength of the corundum peaks increase considerably in moving along this join to more aluminous compositions. We also revisited the diffraction patterns of samples quenched to ambient conditions of Walter et al. [14] in compositions along the $MgSiO_3$–$AlO_{1.5}$ join. Perovskite patterns with no corundum peaks were evident in aluminous compositions with up to 20 mol% $AlO_{1.5}$, but weak corundum peaks were discovered in spectra from the composition with 25 mol% $AlO_{1.5}$. Thus, our new results, together with those of Walter et al. [14], indicate that the maximum solubility of $AlO_{1.5}$ in perovskite should occur close to 25 mol% $AlO_{1.5}$ at conditions of the upper part of the lower mantle. This is in excellent agreement with the results of Ito et al. [31], who located the transition perovskite + corundum ↔ perovskite in pyrope composition (25 mol% $AlO_{1.5}$) at 36–37 GPa at 1600 °C using a sintered diamond cubic–octahedral anvil cell. This result also agrees well with the phase diagram for $MgSiO_3$–$MgAl_2Si_3O_{12}$ at lower mantle pressures as drawn by Kubo and Akaogi [28]. The join $MgSiO_3$–$AlO_{1.5}$ is apparently binary, as we did not observe any stishovite or $MgAl_2O_4$ phase in the experiments with more than 25 mol% $AlO_{1.5}$ (i.e. we did not cross a tie-line between SiO_2 and $MgAl_2O_4$ in highly aluminous compositions along this join).

3.2. Unit cell volumes of perovskite at ambient conditions, V_0

Solution of alumina into perovskite causes distortion of the perovskite lattice and a systematic increase in unit cell volume with increasing alumina content [7,8,14,28–30,32,33]. Measured values of V_0 for perovskites synthesized in our experiments are given in Table 3. We found no evidence for transformation of perovskite to a Li–niobate structured phase upon pressure quench [34]. All unit cell volumes are calculated based on the orthorhombic *Pbnm* space group.

Fig. 5 shows that perovskites synthesized in this study have unit cell volumes with a trend compatible with previous experimental data. Our new data shows volume increasing with $AlO_{1.5}$ at a rate statistically the same as that observed by Walter et al. [14]. However, our new data generally fall below the data of Walter et al. [14]. Error bars on Fig. 5 show precision of the unit cell fitting, and do not include systematic inter-lab differences arising from diffraction calibration. For example, systematic differences in measurement of sample to detector difference of only a few tens of microns can produce differences in cell volume of a few tenths of a cubic angstrom.

Based on our new data combined with data from [14], we find that V_0 of perovskites synthesized along the join $MgSiO_3$–$AlO_{1.5}$ reaches a maximum of about 164.7 Å^3 at ~25 mol% $AlO_{1.5}$. The plateau in V_0 corresponds to the

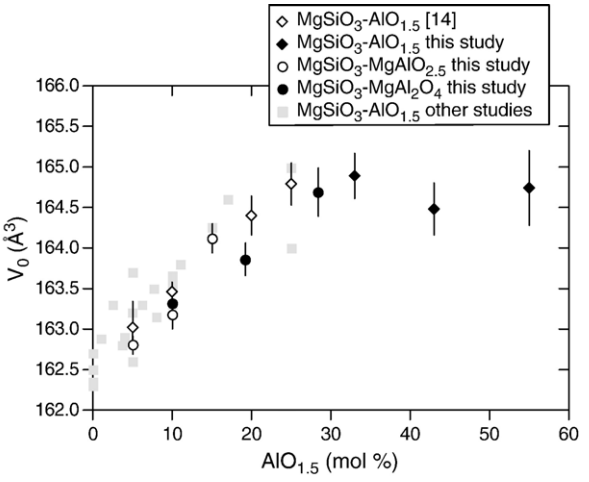

Fig. 5. Ambient unit cell volumes (Å^3) of perovskites synthesized in this study and in the study of Walter et al. [14]. Also shown as lightly shaded squares are unit cell volumes for end member $MgSiO_3$ and aluminous perovskite reported in other studies [4–8,28,29,31,32,40–42]. The plotted $AlO_{1.5}$ contents for samples along the $MgSiO_3$–$AlO_{1.5}$ join are the same as in the bulk compositions. $AlO_{1.5}$ contents of perovskites synthesized along the $MgSiO_3$–$MgAlO_{2.5}$ and $MgSiO_3$–$MgAl_2O_4$ joins are plotted as the median alumina contents between the starting mixtures and the projected alumina contents along the $MgSiO_3$–$AlO_{1.5}$ join (see Fig. 2). We interpret the plateau in cell volume at ~164.7 Å^3 to correlate with a maximum solubility of alumina in perovskite of about 25 mol% $AlO_{1.5}$. Thus, perovskites in samples with higher bulk $AlO_{1.5}$ contents would all plot at about 25 mol% $AlO_{1.5}$.

maximum solubility of $AlO_{1.5}$ in perovskite at the experimental conditions, and is in excellent agreement with the observation noted above that corundum crystallizes in starting compositions with about 25 mol% $AlO_{1.5}$ and greater.

In principle, variation in V_0 can be used as a diagnostic tool for deducing the alumina substitution mechanism along the $MgSiO_3$–$MgAlO_{2.5}$ and $MgSiO_3$–$MgAl_2O_4$ joins. Fig. 6 shows the predicted effect of aluminum substitution mechanism on V_0 (relative to end member $MgSiO_3$ perovskite) of the two substitution reactions based on the *ab initio* calculations of Brodholt [9] and Yamamoto et al. [10]. These calculations show that substitution by the charge-coupled mechanism (reaction (1)) produces a mild increase in cell volume relative to $MgSiO_3$ perovskite. The experimental data of Walter et al. [14] along the charge-coupled join show a generally consistent but somewhat higher rate of increase. In contrast, theoretical calculations show a much greater rate of increase in relative V_0 if alumina substitution occurs by the O-defect forming mechanism (reaction (2)). Also plotted in Fig. 6 are relative changes in

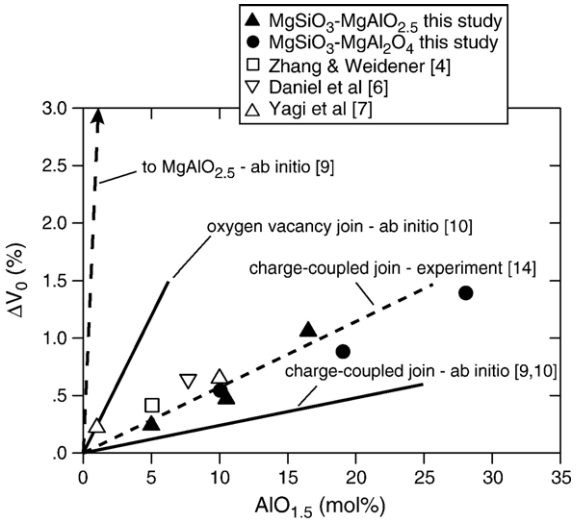

Fig. 6. Change in unit cell volume (ΔV_0 in %) of aluminous perovskites relative to the $MgSiO_3$ perovskite end member (fixed at 162.5 Å^3 for experimental data) as a function of alumina content. $AlO_{1.5}$ contents of perovskites synthesized along the $MgSiO_3$–$MgAlO_{2.5}$ and $MgSiO_3$–$MgAl_2O_4$ joins in this study are plotted as the median alumina contents between the starting mixtures and the projected alumina contents along the $MgSiO_3$–$AlO_{1.5}$ join (see Fig. 2). The long dashed line shows an extrapolation between end member $MgSiO_3$ perovskite and a fictive $MgAlO_{2.5}$ phase based on the *ab initio* calculations of Brodholt [9]. The solid lines show changes in cell volume calculated for the oxygen vacancy and charge-coupled joins based on the *ab initio* calculations of Brodholt [9] and Yamamoto et al. [10] (averaged values from Table 4 of Yamamoto et al. [10]). The short dashed line shows the best linear fit to the experimental data of Walter et al. [14].

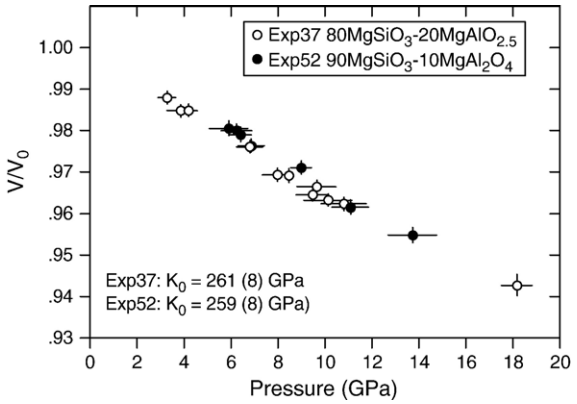

Fig. 7. Relative volume (V/V_0) as a function of pressure for samples Exp37 and Exp52 (see Table 4). Error bars are based on standard error in refined cell parameters of perovskites and the Pt pressure standard. Fitted values of K_0 are 261±8 and 259±8 for Exp37 and Exp52, respectively, assuming that the pressure derivative, $K'=4$. Error in K_0 based on standard error in the nonlinear least-squares regression.

V_0 observed in our experiments along the $MgSiO_3$–$MgAlO_{2.5}$ and $MgSiO_3$–$MgAl_2O_4$ joins. It is clear that the volume changes correspond closely to the rate of increase expected for the charge-coupled substitution mechanism, but fall far below relative volumes predicted from theory if single-phase O-defect perovskite is stable along the $MgSiO_3$–$MgAlO_{2.5}$ join. This evidence further corroborates our deduction from phase relations that alumina substitution into perovskite along the two MgO-rich joins is dominated by charge-coupled substitution.

Also shown in Fig. 6 are changes in relative volume for a set of unusually compressive aluminous perovskites [4,6,7]. These perovskites have ambient unit cell volumes that are consistent with charge-coupled substitution. If the unusual softness of these perovskites were due to incorporation of oxygen vacancies as postulated previously [4,6,14,17], and if theory is a useful guide, we would have expected these perovskites to have unusually large unit cell volumes, which they do not. However, we note that in all cases the unusually compressive perovskites were synthesized from starting mixtures along the charge-coupled join, $MgSiO_3$–$AlO_{1.5}$. We have shown that the charge-coupled substitution component is stable along this join up to ~25 mol% $AlO_{1.5}$, so the unit cell volumes of these perovskites are consistent with the phase relations. Apparently, the unusual compressibility measurements are not a consequence of oxygen vacancy formation.

3.3. Compressibility

We measured the room-temperature compressibility of two synthesized samples, Exp37 (80$MgSiO_3$–

Table 4
Unit cell volumes, cell parameters, and calculated pressures in compression experiments

	Sample #	V_{Pt} (Å^3)	P [a] (GPa)	V_{Pv} (Å^3)	a (Å)	b (Å)	c (Å)
Exp37	Ambient	–	10^{-4}	163.18 (9)	4.7771 (17)	4.9385 (14)	6.9167 (23)
	37.01	59.68 (8)[b]	3.26 (38)	161.22 (16)	4.7640 (19)	4.9167 (21)	6.8830 (55)
	37.04	59.56 (11)	3.84 (55)	160.71 (13)	4.7528 (21)	4.9119 (19)	6.8840 (38)
	37.03	59.49 (8)	4.17 (39)	160.72 (15)	4.7562 (20)	4.9137 (18)	6.8771 (51)
	37.06	58.97 (11)	6.79 (56)	159.28 (16)	4.7364 (23)	4.9013 (26)	6.8611 (47)
	37.07	58.75 (12)	7.96 (63)	158.19 (16)	4.7323 (24)	4.8915 (19)	6.8338 (54)
	37.08	58.66 (3)	8.45 (16)	158.16 (17)	4.7258 (26)	4.8895 (25)	6.8450 (50)
	37.10	58.44 (15)	9.63 (83)	157.72 (16)	4.7213 (26)	4.8841 (26)	6.8398 (51)
	37.09	58.47 (13)	9.46 (69)	157.41 (17)	4.7212 (23)	4.8812 (29)	6.8303 (51)
	37.11	58.35 (19)	10.12 (102)	157.19 (14)	4.7143 (21)	4.8820 (20)	6.8298 (42)
	37.12	58.23 (17)	10.79 (96)	157.04 (15)	4.7140 (21)	4.8810 (21)	6.8250 (48)
	37.15	57.00 (10)	18.16 (65)	153.85 (34)	4.6818 (49)	4.8575 (37)	6.7649 (119)
Exp52	Ambient	–	10^{-4}	163.26 (9)	4.7793 (13)	4.9369 (9)	6.9192 (17)
	52.03	59.15 (16)	5.89 (82)	159.79 (21)	4.7481 (28)	4.9031 (21)	6.8639 (76)
	52.01	59.19 (23)	6.23 (65)	159.77 (15)	4.7452 (25)	4.9017 (20)	6.8691 (45)
	52.04	59.09 (19)	6.39 (47)	159.55 (20)	4.7440 (34)	4.8972 (27)	6.8677 (62)
	52.05	58.96 (12)	6.85 (56)	159.13 (18)	4.7410 (27)	4.8981 (20)	6.8529 (61)
	52.06	58.59 (16)	8.97 (43)	158.27 (18)	4.7344 (31)	4.8860 (21)	6.8419 (59)
	52.08	58.18 (22)	11.07 (78)	156.71 (19)	4.7165 (28)	4.8742 (21)	6.8168 (64)
	52.09	57.72 (18)	13.72 (103)	155.61 (20)	4.7040 (31)	4.8636 (23)	6.8017 (70)

[a] Pressure calculated from equation of state for Pt of Holmes [28].
[b] Error in least significant digits based on standard error in unit cell refinement.

$20MgAlO_{2.5}$) and Exp52 ($90MgSiO_3$–$10MgAl_2O_4$). Fig. 7 shows compression curves for these two samples measured at pressures between 1 atm and ~18 GPa. We fitted these data to the 3rd-order Birch–Murnaghan equation of state in order to determine the room temperature bulk modulus, K_0, assuming a value for the pressure derivative of the bulk modulus, K', of 4.0. Unit cell data along with regression data are provided in Table 4. The ambient bulk moduli, K_0, obtained from these samples are 261±8 and 259±8 GPa for Exp37 and Exp52, respectively. These values are, within uncertainty, equivalent to the bulk modulus of $MgSiO_3$ perovskite, and fall within uncertainty of K_0 measured for aluminous perovskites along the charge-coupled join, $MgSiO_3$–$AlO_{1.5}$ [14]. These perovskites are not considerably more compressive than end member $MgSiO_3$ perovskite as predicted for O-defect perovskite in theoretical calculations [9,10,12]. Thus, these results are consistent with our observations from phase relations and the systematics of V_0 that alumina substitution into perovskites synthesized along the $MgSiO_3$–$MgAlO_{2.5}$ and $MgSiO_3$–$MgAl_2O_4$ joins is predominantly by the charge-coupled reaction.

Fig. 8 shows values of K_0 for perovskite as a function of alumina content as measured in this and other studies. K_0 values appear to fall into two groups. One group of higher values that show a mild decrease in K_0 with increasing alumina content, and another group of lower values, which can also be interpreted to show a mild decrease in K_0 with alumina content for concentrations of 1 mol% alumina and greater. Yagi et al. [7] measured a bulk modulus for a perovskite with only 1 mol% $AlO_{1.5}$ that is much lower than measured values of $MgSiO_3$ perovskite, but is only nominally larger than K_0 measured for perovskites with 5 to 10 mol% alumina in the lower K_0 group [4–6]. The decrease in bulk modulus due to

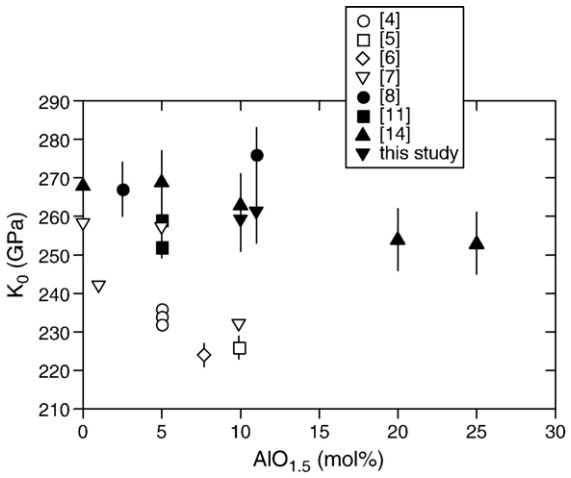

Fig. 8. The ambient (300 K) bulk modulus of perovskite, K_0, as a function of alumina content (mol%) from experimental data in this and other studies. The pressure derivative of the bulk modulus, K', is assumed to be 4 in all cases.

incorporation of alumina into perovskite along the oxygen vacancy join, $MgSiO_3$–$MgAlO_{2.5}$, is predicted to be non-linear [9,10], but not to the extreme extent indicated by the results of Yagi et al. [7]. We reiterate that all the starting mixtures in the group with low K_0 values were nominally along the charge-coupled join. It is difficult to fathom how equilibrium perovskites with considerable oxygen vacancies could have formed in such compositions given that the charge-coupled substitution component is stable along the $MgSiO_3$–$AlO_{1.5}$ join up to about 25 mol% alumina. Also, our new experimental results and the theoretical calculations of Akber-Knutsen and Bukowinski [12] indicate that defect perovskites are not stable along the oxygen vacancy join at mantle conditions. We conclude that the lower K_0 values are not likely due to alumina substitution by the vacancy forming reaction, but that another cause is implicated.

Recent results show that the low K_0 values reported for aluminous perovskite are not entirely reproducible (Fig. 8). Daniel et al. [11] measured K_0 for a perovskite with 5 mol% alumina that is 10% to 15% higher than measured previously for a composition with 7.7% alumina by Daniel et al. [6], although the experimental methodology was similar. Yagi et al. [7], in a single study, measured values of K_0 that fall within both the higher K_0 group and the lower K_0 group, with the differences well outside the reported uncertainties. Yagi et al. [7] and Walter et al. [14] have discussed the difficulty in identifying unifying factors common within the two groups of K_0 values. The only commonality among the lower group of values is that in all cases the perovskites used in the compression studies were quenched from high pressure and temperature, removed from their initial experimental containers, and placed within a second experimental charge. It is conceivable that treatment of the perovskites could have lead to partial amorphization and softening of the structures [7]. However, we note that in the present study, as well as in the study of Daniel et al. [11], a similar methodology was adopted but high values of K_0 were measured. A definitive explanation for the unusual compressibility of some aluminous perovskites remains elusive.

4. Discussion

We have presented three lines of evidence indicating that substitution of alumina into the perovskite structure occurs predominantly by charge-coupled substitution, even for starting compositions along the MgO-saturated join $MgSiO_3$–$MgAlO_{2.5}$ (the O-defect join) and the $MgSiO_3$–$MgAl_2O_4$ join. Firstly, the phase identification of run products indicates the presence of periclase co-existing with perovskite. Secondly, the ambient unit cell volumes are consistent with those observed and calculated for charge-coupled substitution. Thirdly, the compressibilities of perovskites synthesized along these joins are not anomalously low relative to the $MgSiO_3$ perovskite end member. Computational mineral physics studies generally predict significantly expanded unit cell volumes and correspondingly increased compressibilities for hypothetical O-defect aluminous $MgSiO_3$-based perovskites (e.g. [9,10]).

Navrotsky et al. [17] and Walter et al. [14] suggested that because of the MgO-rich nature of primitive mantle peridotite, solubility of defects into perovskite could have important consequences for the mantle, especially given that both experimental and theoretical studies had indicated the large effect defects could have on compressibility. Based on our results, we have drawn a phase diagram for the system MgO–$AlO_{1.5}$–SiO_2 appropriate for conditions of the upper part of the lower mantle as shown in Fig. 9. Although there is uncertainty in pressure because we could not place a ruby grain in the center of the sample itself, estimates of pressure based on calibration runs indicate that this phase diagram is appropriate for

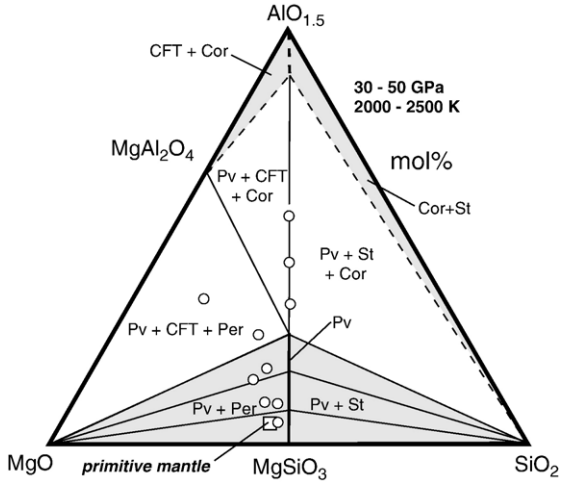

Fig. 9. Generalized phase relations in the system MgO–$AlO_{1.5}$–SiO_2 (mol%) for the upper part of the lower mantle. The maximum solubility of alumina in perovskite occurs at ~25 mol% $AlO_{1.5}$. The join $MgSiO_3$–$AlO_{1.5}$ is considered binary, as only perovskite and corundum were observed in the three experiments along this join with more than 25 mol% $AlO_{1.5}$ in the starting composition. Shaded areas show two-phase regions where aluminous perovskite solid solution (Pv) coexists with either periclase (Per) or stishovite (St), and corundum solid solution (Cor) coexists with either stishovite or a high pressure form of $MgAl_2O_4$ (CFT=calcium ferrite or calcium titanate structure). Three-phase regions include Pv+CFT+Per, Pv+CFT+Cor, and Pv+St+Cor. Circles show bulk composition used in this study. The square shows a pyrolitic primitive mantle composition projected into this system.

pressures in the range of 30–50 GPa and temperatures of 2000–2500 K. We interpret our results to indicate very limited solubility of O-defects at these conditions, consistent with the theoretical results of Akber-Knutsen and Bukowinski [12], and so we presume that alumina substitutes into perovskite almost entirely along the charge coupled join $MgSiO_3$–$AlO_{1.5}$. The solubility limit along the charge-coupled join is placed at ~25 mol% $AlO_{1.5}$, consistent with the results of Ito et al. [31], and the solubility of alumina in perovskite may increase with pressure [28]. The join $MgSiO_3$–$AlO_{1.5}$ is apparently binary and some solution of $MgSiO_3$ is expected in corundum as well.

Primitive mantle compositions projected into the MAS-system plot very close to the $MgSiO_3$–$MgAlO_{2.5}$ join in Fig. 9. The lever rule indicates about 90 mol% perovskite with ~5 mol% $AlO_{1.5}$ coexisiting with ~10 mol% periclase for the primitive mantle composition. The perovskite is expected to have a bulk modulus only a few percent lower than the $MgSiO_3$ perovskite end member. Given that O-defects are disfavored by pressure [9,10,12], the general form of this phase diagram may be generally applicable throughout the lower mantle pressure range to the limit of perovskite stability. The possible exception is at shallower pressures not investigated in this study (e.g. 25–30 GPa). However, we find it unlikely that defects are important even in this regime, because theory indicates very limited solubility of defects throughout the lower mantle pressure–temperature range [12], and because the alumina content of perovskite is low in this pressure range due to the coexistence of majorite garnet [28,31,32].

The remaining question is how the presence of ferric iron affects the phase relations. Experiments indicate that aluminous perovskites can accommodate a large and often dominant proportion of the total iron as Fe^{3+} [35–37]. Substitution reactions analogous to the charge-coupled and defect components can also be written for Fe^{3+}. Correlation of Al^{3+} and Fe^{3+} indicates coupled substitution of these elements [35,38]. Recent single-crystal data on alumina and iron-bearing (ferric and ferrous) perovskites show that substitution of these cations is accomplished primarily through a charge-coupled reaction where Al substitutes for Si on the octahedral site and Fe for Mg on the larger 8-fold site [16], confirming earlier predictions. Theoretical results also show that charge-coupled substitution is favored for ferric iron [39]. Thus, it appears that the defect forming reaction will not be important for perovskite in natural mantle compositions. However, determination of the solubility limit of Fe^{3+} and its effect on elastic properties along joins analogous to those studied here awaits experimental verification at lower mantle conditions.

5. Conclusions

We have determined the phase relations of aluminous perovskite in the system MgO–Al_2O_3–SiO_2 at conditions of the upper part of the lower mantle. Synthesis experiments made in the laser-heated diamond anvil cell for compositions along the MgO-saturated join $MgSiO_3$–$MgAlO_{2.5}$ (O-defect join) and $MgSiO_3$–$MgAl_2O_4$ demonstrate the coexistence of perovskite and periclase, indicating an insignificant proportion of the O-defect forming substitution. These results seem to indicate that perovskites crystallizing from compositions in the MgO-rich portion of the diagram have compositions along or very close to the $MgSiO_3$–$AlO_{1.5}$ join (the charge-coupled join). The maximum solubility of alumina in perovskite along the $MgSiO_3$–$AlO_{1.5}$ join is ~25 mol%, and the join appears to be binary. Unit cell volumes of perovskites synthesized from compositions along the MgO-rich joins are consistent with those measured and calculated for perovskites crystallizing along the charge-coupled join. We measured the compressibility of perovskites synthesized from starting compositions along the $MgSiO_3$–$MgAlO_{2.5}$ and $MgSiO_3$–$MgAl_2O_4$ joins and found bulk moduli comparable to previous measurements and predictions for aluminous perovskites along the charge-coupled join. These bulk moduli are considerably larger than those predicted from computational mineral physics for oxygen-defect perovskite.

Our results indicate that alumina substitution into perovskite occurs primarily by a charge-coupled reaction throughout the lower mantle, with very limited substitution by an O-defect forming reaction. MgO-rich compositions like primitive mantle will crystallize aluminous perovskite (~5 mol% $AlO_{1.5}$) coexisting with periclase. In natural Fe-bearing mantle peridotite the corresponding coexisting phase will be ferropericlase. The compressibility of aluminous perovskite along the charge-coupled substitution join seems to be only a few percent lower than for end member $MgSiO_3$ perovskite [9,10,12,14]. The perovskites crystallizing from natural mantle compositions are expected to contain the equivalent charge-coupled substitution component Fe^{3+} AlO_3. Further studies are needed explore the phase relations and elastic properties of perovskites containing ferrous and ferric iron in addition to aluminum.

Acknowledgements

The authors thank M. Kunz for excellent assistance at ALS beamline 12.2.2. Comments from two anonymous reviewers were very helpful in improving the manuscript. This work was supported by NERC grant

NE/C506921/1 awarded to MJW and Nansen Foundation grant 45/2005 from the Norwegian Academy of Science and Letters to RGT.

References

[1] C.R. Bina, P.G. Silver, Constraint on lower mantle composition and temperature from density and bulk sound velocity profiles, Geophys. Res. Lett. 17 (1990) 1153–1156.

[2] I. Jackson, S.M. Rigden, Composition and temperature of the Earth's mantle: seismological models interpreted through experimental studies of Earth materials, in: I. Jackson (Ed.), The Earth's Mantle: Composition, Structure and Evolution, Cambridge University Press, Cambridge, UK, 1998, pp. 405–460.

[3] T. Yagi, N. Funamori, Chemical composition of the lower mantle inferred from the equation of state of $MgSiO_3$ perovskite, Philos. Trans. R. Soc. Lond. Ser. A: Math. Phys. Sci. 354 (1996) 1371–1384.

[4] J. Zhang, D.J. Weidener, Thermal equation of state of aluminum-enriched silicate perovskite, Science 284 (1999) 782–784.

[5] A. Kubo, T. Yagi, S. Ono, M. Akaogi, Compressibility of $Mg_{0.9}Al_{0.2}Si_{0.9}O_3$ perovskite, Proc. Jpn. Acad. 76B (2000) 103–107.

[6] I. Daniel, H. Cardon, G. Fiquet, F. Guyot, M. Mezouar, Equation of state of Al-bearing perovskite to lower mantle conditions, Geophys. Res. Lett. 28 (2001) 3789–3792.

[7] T. Yagi, K. Okabe, N. Nishiyama, A. Kubo, T. Kikegawa, Complicated effects of aluminum on the compressibility of silicate perovskite, Phys. Earth Planet. Inter. 143–144 (2004) 81–89.

[8] D. Andrault, N. Bolfan-Casanova, N. Guignot, Equation of state of lower mantle (Al,Fe)–$MgSiO_3$ perovskite, Earth Planet. Sci. Lett. 193 (2001) 501–508.

[9] J.P. Brodholt, Pressure-induced changes in the compression mechanism of aluminous perovskite in the Earth's mantle, Nature 407 (2000) 620–622.

[10] T. Yamamoto, D.A. Yuen, T. Ebisuzaki, Substitution mechanism of Al ions in $MgSiO_3$ perovskite under high pressure conditions from first-principles calculations, Earth Planet. Sci. Lett. 206 (2003) 617–625.

[11] I. Daniel, J.D. Bass, G. Fiquet, H. Cardon, J. Zhang, M. Hanfland, Effect of aluminum on the compressibility of silicate perovskite, Geophys. Res. Lett. 31 (2004), doi:10.1029/2004GL020213.

[12] S. Akber-Knutsen, M.S.T. Bukowinski, The energetics of aluminum solubility into $MgSiO_3$ perovskite at lower mantle conditions, Earth Planet. Sci. Lett. 220 (2004) 317–330.

[13] S. Ono, T. Kikegawa, T. Iizuka, The equation of state of orthorhombic perovskite in a peridotitic mantle composition to 80 GPa: implication for chemical composition of the lower mantle, Phys. Earth Planet. Inter. (2005) 9–17.

[14] M. Walter, A. Kubo, T. Yoshino, J. Brodholt, K.T. Koga, Y. Ohishi, Phase relations and equation-of-state of aluminous Mg–silicate perovskite and implications for Earth's lower mantle, Earth Planet. Sci. Lett. 222 (2004) 501–516.

[15] J.M. Jackson, J. Zhang, J. Shu, S.V. Sinogeikin, J.D. Bass, High-pressure sound velocities and elasticity of aluminous $MgSiO_3$ perovskite to 45 GPa: implications for lateral heterogeneity in Earth's lower mantle, Geophys. Res. Lett. 32 (2005), doi:10.1029/2005GL023522.

[16] C.B. Vanpeteghema, R.J. Angel, N.L. Ross, S.D. Jacobsen, D.P. Dobsonc, K.D. Litasov, E. Ohtani, Al,Fe substitution in the $MgSiO_3$ perovskite structure: a single-crystal X-ray diffraction study, Phys. Earth Planet. Inter. 155 (2006) 96–103.

[17] A. Navrotsky, M. Schoenitz, H. Kojitani, H. Xu, J. Zhang, D.J. Weidener, R. Jeanloz, Aluminum in magnesium silicate perovskite: formation, structure, and energetics of magnesium-rich defect solid solutions, J. Geophys. Res. 108 (2003) 2330, doi:10.1029/102002JB002055.

[18] N.C. Richmond, J.P. Brodholt, Calculated role of aluminum in the incorporation of ferric iron into magnesium silicate perovskite, Am. Mineral. 83 (1998) 947–951.

[19] J.P. Brodholt, A.R. Oganov, G.D. Price, Computational mineral physics and the physical properties of perovskite, Philos. Trans. R. Soc. Lond. 360 (2002) 2507–2520.

[20] J.A. Peck, I. Farnan, J.F. Stebbins, Disordering and the progress of hydration at the surface of diopside: a cross polarization MAS–NMR study, Geochim. Cosmochim. Acta 52 (1988) 3017–3021.

[21] H.K. Mao, J. Xu, P.M. Bell, Calibration of the ruby pressure gauge to 800 kbar under quasi-hydrostatic conditions, J. Geophys. Res. 91 (1986) 4673–4676.

[22] W.R. Panero, R. Jeanloz, Temperature gradients in the laser-heated diamond anvil cell, J. Geophys. Res. 106 (2001) 6493–6498.

[23] G. Shen, M.L. Rivers, Y. Wang, S.R. Sutton, Laser heated diamond cell system at the advanced photon source for in situ X-ray measurements at high pressure and temperature, Rev. Sci. Inst. 72 (2001) 1273–1282.

[24] M.J. Walter, K.T. Koga, The effects of chromatic dispersion on temperature measurement in the laser-heated diamond anvil cell, Phys. Earth Planet. Inter. 143–144 (2004) 541–558.

[25] A.P. Hammersley, FIT2D: an introduction and overview, Technical Report ESRF-97-HA-02T, ESRF, Grenoble, 1997.

[26] U.D. Altermatt, I.D. Brown, A real-space computer-based symmetry algebra, Acta Crystallogr. A43 (1987) 125–130.

[27] N.C. Holmes, J.A. Moriarty, G.R. Gathers, W.J. Nellis, The equation of state of platinum to 660 GPa (6.6 Mbar), J. Appl. Phys. 66 (1989) 2962–2967.

[28] A. Kubo, M. Akaogi, Post-garnet transitions in the system $Mg_4Si_4O_{12}$–$Mg_3Al_2Si_3O_{12}$ up to 28 GPa: phase relations of garnet, ilmenite and perovskite, Phys. Earth Planet. Inter. 121 (2000) 85–102.

[29] K. Weng, H.K. Mao, P.M. Bell, Lattice parameters of the perovskite phase in the system $MgSiO_3$–$CaSiO_3$–Al_2O_3, Carnegie Inst. Washington, Year Book, vol. 81, 1982, pp. 273–277.

[30] N. Funamori, R. Jeanloz, J. Nguyen, A. Kavner, W. Caldwell, K. Fujino, N. Miyajima, T. Shinmei, N. Tomioka, High-pressure transformations in $MgAl_2O_4$, J. Geophys. Res. 103 (1998) 20, 813–820,818.

[31] E. Ito, A. Kubo, T. Katsura, M. Akaogi, T. Fujita, High-pressure transformation of pyrope $Mg_3Al_2Si_3O_{12}$ in a sintered diamond cubic anvil assembly, Geophys. Res. Lett. 25 (1998) 821–824.

[32] T. Irifune, T. Koizumi, J.-I. Ando, An experimental study of the garnet–perovskite transformation in the system $MgSiO_3$–$Mg_3Al_2Si_3O_{12}$, Phys. Earth Planet. Inter. 96 (1996) 147–157.

[33] B. O'Neill, R. Jeanloz, $MgSiO_3$–$FeSiO_3$–Al_2O_3 in the Earth's lower mantle: perovskite and garnet at 1200 km depth, J. Geophys. Res. 99 (1994) 19,901–19,915.

[34] N. Funamori, T. Yagi, N. Miyajima, K. Fujino, Transformation in garnet: from orthorhombic perovskite to $LiNbO_3$ phase on release of pressure, Science 275 (1997) 513–515.

[35] D.J. Frost, F. Langenhorst, The effect of Al_2O_3 on Fe–Mg partitioning between magnesiowustite and magnesium silicate perovskite, Earth Planet. Sci. Lett. 199 (2002) 227–241.

[36] S. Lauterbach, C.A. McCammon, P.V. Aken, F. Langenhorst, F. Seifert, Mossbauer and ELNES spectroscopy of (Mg,Fe)(Si,Al)

O_3 perovskite: a highly oxidized component of the lower mantle, Contrib. Mineral. Petrol. 138 (2000) 17–26.
[37] C. McCammon, Perovskite as a possible sink for ferric iron in the lower mantle, Nature 387 (1997) 694–696.
[38] B.J. Wood, D.C. Rubie, The effect of alumina on phase transformations at the 660-km discontinuity from Fe–Mg partitioning experiments, Science 273 (1996) 1522–1524.
[39] L. Li, J.P. Brodholt, S. Stackhouse, D.J. Weidner, M. Alfredsson, G.D. Price, Elasticity of (Mg,Fe)(Si,Al)O_3–perovskite at high pressure, Earth Planet. Sci. Lett. 240 (2005) 529–536.
[40] G. Fiquet, D. Andrault, A. Dewaele, T. Charpin, M. Kunz, D. Hauserman, *P–V–T* equation of state of $MgSiO_3$ perovskite, Phys. Earth Planet. Inter. 105 (1998) 21–31.
[41] N. Funamori, T. Yagi, W. Utsumi, T. Kondo, T. Uchida, Thermoelastic properties of $MgSiO_3$ perovskite determined by in situ X ray observations up to 30 GPa and 2000 K, J. Geophys. Res. 101 (1996) 8257–8269.
[42] H.K. Mao, R.J. Hemley, Y. Fei, J.F. Shu, L.C. Chen, A.P. Jephcoat, Y. Wu, W.A. Bassett, Effect of pressure, temperature, and composition on lattice parameters and density of (Fe,Mg)SiO_3–perovskites to 30 GPa, J. Geophys. Res. 96 (1991) 8069–8079.